Mathematical modelling of calcium binding in solution

Bachelor thesis

Student: Mirtel Toming
Student code: 233465YAFB
Supervisors: Marko Vendelin, Professor
Maike Mona Širinov, Early Stage Researcher
Laboratory of Systems Biology
Study program: Applied Physics

Tallinn 2026

Kaltsiumi seondumise matemaatiline modelleerimine lahuses

Bakalaureusetöö

Üliõpilane: Mirtel Toming
Üliõpilaskood: 233465YAFB
Juhendajad: Marko Vendelin, professor
Maike Mona Širinov, doktorant-nooremteadur
Süsteemibioloogia labor
Küberneetika instituut
Õppekava: Rakendusfüüsika

Tallinn 2026

Declaration

I hereby declare that I have written this thesis independently and the thesis has not previously been submitted for defence. All works and major viewpoints of the other authors, data from sources of literature and elsewhere used for writing this paper have been properly cited.

Author: Mirtel Toming

The thesis complies with the requirements for bachelor's theses
Supervisors:

Marko Vendelin

Maike Mona Širinov

Contents

Abstract

For accurate force–calcium measurements in cardiac muscle preparations, it is essential to know the free calcium concentration of the bathing solution. Free calcium is buffered with the chelator EGTA and measured with a fluorescent calcium indicator, both of which rely on dissociation constants typically taken from tables or manufacturer data. These values depend on pH, ionic strength, temperature, and chelator purity, and can deviate substantially from the actual values under experimental conditions.

The aim of this work was to develop a fluorescence-based calibration procedure that determines the relevant dissociation constants under the buffer conditions used for force measurements, so that free calcium in such solutions can be calculated reliably from known total concentrations.

The first part of this thesis gives a general overview of cardiac muscle structure and function, excitation–contraction coupling, force measurements in permeabilized preparations, and the principles of fluorescence and calcium chelators. The subsequent sections describe the mathematical model and the experiments conducted in this study and present the corresponding results.

A model of the dye–EGTA–calcium equilibrium and a fitting procedure were developed, verified against synthetic data, and applied to measured fluorescence data. The fitted curves matched the measured data across varied conditions.

This procedure will be further developed to support calibration of free calcium in solutions used for cardiac muscle force measurements.

Annotatsioon

Täpsete jõu–kaltsiumi mõõtmiste tegemiseks südamelihase preparaatides on oluline teada ümbritseva lahuse vaba kaltsiumi kontsentratsiooni. Vaba kaltsiumi puhverdatakse kelaatoriga ja mõõdetakse fluorestseeruva kaltsiumi indikaatoriga, mõlemad tuginevad dissotsiatsioonikonstantidele, mis tavaliselt võetakse kirjandusest või tootja andmetest. Need väärtused sõltuvad aga pH-st, ioontugevusest, temperatuurist ja kelaatori partii kvaliteedist ning võivad eksperimentaalsetes tingimustes tegelikest väärtustest oluliselt erineda.

Käesoleva töö eesmärk oli välja töötada fluorestsentsil põhinev kalibreerimisprotseduur, mis määrab vastavad dissotsiatsioonikonstandid jõu mõõtmistel kasutatava puhvri tingimustes, nii et vaba kaltsiumi kontsentratsiooni sellistes lahustes saaks teadaolevatest väärtustest usaldusväärselt arvutada.

Töö esimeses osas antakse üldine ülevaade südamelihase struktuurist ja funktsioonist, elektromehaanilisest sidestusest, jõu mõõtmistest permeabiliseeritud preparaatides ning fluorestsentsi ja kaltsiumi kelaatorite põhimõtetest. Järgnevates osades kirjeldatakse käesolevas töös kasutatud matemaatilist mudelit ja teostatud katseid ning esitatakse vastavad tulemused.

Töötati välja kaltsiumi seondumise mudel ja sobitusmeetod, mida kontrolliti sünteetiliste andmete põhjal ning rakendati mõõdetud fluorestsentsi andmetele. Sobitatud kõverad ühtisid erinevates tingimustes mõõdetud andmetega.

Seda meetodit arendatakse edasi, et võimaldada täpsemat vaba kaltsiumi kontsentratsiooni määramist südamelihase preparaatide jõu mõõtmiseks kasutatavates lahustes.

Introduction

The heart pumps blood by repeated contraction of its muscle cells, the cardiomyocytes. Each contraction is triggered by a rise in the free calcium concentration inside the cell. Calcium binds to a protein on the contractile filaments and allows the filaments to generate force, so the amount of force produced depends on how much free calcium is present.

To study how calcium controls force, cardiomyocytes and myofibrils can be permeabilized and placed in solutions with a chosen free calcium concentration. The concentrations of interest are very low, in the sub-micromolar range, so they cannot be set by adding a known amount of calcium alone: small amounts of contamination or pipetting error shift the free concentration significantly. The solutions are therefore buffered with a calcium chelator such as EGTA, which binds most of the added calcium and holds the free concentration at a stable level. The total amount of calcium needed to reach a desired free concentration is calculated from the dissociation constant of EGTA using software such as MaxChelator or PyChelator.

The free calcium concentration in the buffered solution can be determined by adding a fluorescent calcium indicator, a dye that becomes brighter when it binds calcium. Converting the measured fluorescence into a free calcium concentration requires the dissociation constant of the dye, $K_{d,\mathrm{Dye}}$, under the same buffer conditions.

Both constants present the same problems. Tabulated values depend on pH, ionic strength, and temperature, and different sources give different numbers. The chelators are not perfectly pure, and other components of the solution can carry trace amounts of calcium. The manufacturer-reported K_d of the dye has also been shown to differ substantially from the value measured in real buffer conditions.

This thesis develops a mathematical model of the dye–EGTA–calcium equilibrium aimed at determining both dissociation constants from a titration experiment in which EGTA, dye, and calcium are all present in the same solution. The model describes how the dye and EGTA bind calcium and how the dye's fluorescence depends on the amount of bound calcium. It is used both to design the experiment and to recover the dissociation constants from the measured data. It is validated against synthetic data and then applied to a set of fluorescence titration measurements. The work is carried out in support of the ongoing single myofibril force measurements in the laboratory, for which reliable free calcium calibration is necessary.

1. Theoretical background

1.1. Structure and function of cardiac muscle

Cardiac muscle, or myocardium, forms the muscular wall of the heart. It is made up of branching, interconnected muscle cells called cardiomyocytes. Each cardiomyocyte contains many myofibrils, which are in turn made of aligned units called sarcomeres. Sarcomeres are the contractile units of muscle and consist of thick and thin filaments that slide past each other during contraction. Thin filaments are composed of actin, tropomyosin, and the troponin complex, while thick filaments are made of myosin, which has a long tail and a globular head. The regular arrangement of these filaments gives cardiac muscle its characteristic striated appearance as seen in Figure 1.

The troponin complex on the thin filament is the calcium sensor of the sarcomere and consists of three subunits: troponin T (TnT), which anchors the complex to tropomyosin; troponin I (TnI), which inhibits the actin–myosin interaction in the absence of calcium; and troponin C (TnC), which binds Ca^{2+}. When Ca^{2+} binds to TnC, the troponin complex undergoes a conformational change that shifts tropomyosin away from the myosin binding sites on actin, allowing myosin heads to bind and form force-generating cross-bridges. The amount of force a sarcomere produces therefore depends directly on the cytosolic free calcium concentration $[\mathrm{Ca}^{2+}]_i$.

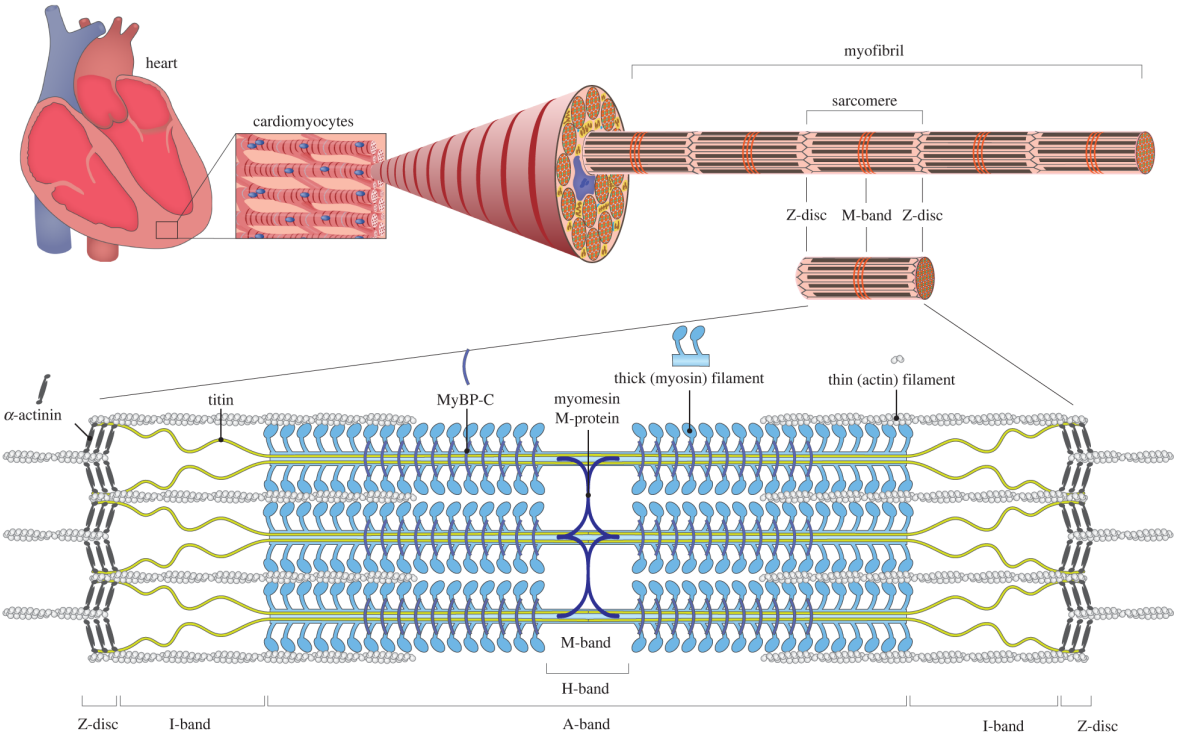

Figure 1: Hierarchical structure of cardiac muscle: heart, cardiomyocyte, myofibril, and sarcomere. The sarcomere consists of thick (myosin) and thin (actin, tropomyosin, troponin) filaments. Reproduced from [1] under CC BY 4.0.

1.2. Excitation–contraction coupling

The link between electrical excitation of a cardiomyocyte and its mechanical contraction is known as excitation–contraction coupling. Each contraction begins with an action potential that depolarises the cell membrane and opens voltage-gated L-type calcium channels in the sarcolemma. A small inward Ca^{2+} current enters the cell and triggers the release of a much larger amount of Ca^{2+} from the sarcoplasmic reticulum (SR) through ryanodine receptors. This process is called calcium-induced calcium release [2, 3].

The combined Ca^{2+} influx and SR release raise the cytosolic free calcium concentration $[\mathrm{Ca}^{2+}]$ from a resting level of about 100 nM to roughly 1 µM during the peak of the transient. At this elevated level, Ca^{2+} binds to troponin C and activates the contractile machinery. For relaxation to follow, $[\mathrm{Ca}^{2+}]$ must return to its resting value. Calcium is removed from the cytosol by four pathways: re-uptake into the SR by SR Ca^{2+}-ATPase, extrusion across the sarcolemma by the Na^{+}/Ca^{2+} exchanger and the sarcolemmal Ca^{2+}-ATPase, and uptake into mitochondria [3]. The schematic of the process is shown in Figure 2.

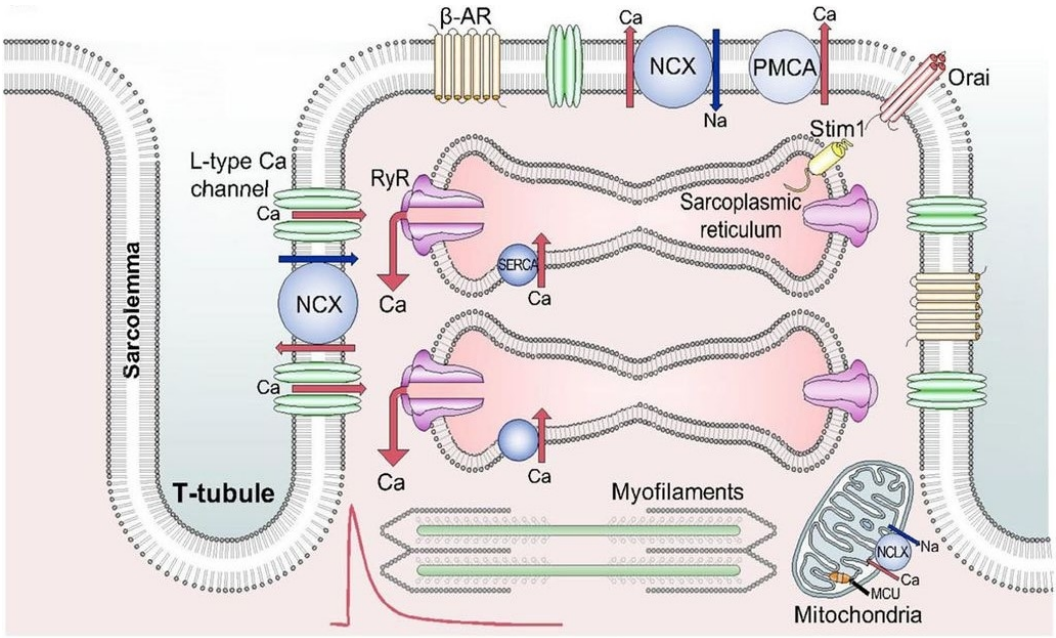

Figure 2: Schematic of excitation–contraction coupling in a ventricular cardiomyocyte showing the surface membrane, T-tubule, sarcoplasmic reticulum, mitochondria, and the channels and transporters involved in Ca^{2+} cycling. Reproduced from Eisner et al. (2017) [4], panel A, under CC BY 4.0.

The amplitude and time course of the calcium transient determine the strength and duration of each heartbeat. Disturbances in calcium handling are linked to heart failure, arrhythmias, and cardiomyopathies [3, 5, 6, 7], which makes accurate measurement of intracellular calcium important for studying cardiac function.

1.3. Force measurements in permeabilized cardiac preparations

Force measurements in permeabilized cardiomyocyte preparations can be performed across a range of structural levels, from single cells to isolated myofibrils. At the single-cell scale, the carbon fiber technique has been established to attach fibers to the ends of an individual cardiomyocyte and record force during contraction, allowing energetic and mechanical parameters to be assessed under controlled resting and contractile loads [8, 9]. To complement these measurements, an image-based method for the real-time determination of sarcomere length during contraction was developed in the same group, enabling sarcomere kinetics to be tracked in parallel with the force recording [10]. Because permeabilization gives direct control over the bathing solution, the contractile apparatus can be exposed to defined calcium concentrations and metabolite levels, which is essential for separating regulation at the myofilament level from cellular and organelle-level processes [11].

Moving below the single-cell scale, isolated myofibrils provide an even more reduced preparation: they are stripped of other cellular systems and their small diameter minimises diffusion-related delays, so changes in calcium reach the contractile filaments almost immediately and the measured force kinetics reflect the contractile machinery itself. Single myofibril force measurements use glass microneedles as deflecting force sensors [12]. Common to all of these preparations is the requirement to expose the contractile apparatus to precisely known free calcium concentrations. Free calcium in this range cannot be controlled by adjusting the total amount of added calcium alone, since the bulk of it binds to chelators and other components of the solution, and the free fraction is set by the resulting binding equilibria. Computational tools such as MaxChelator estimate this free fraction from the total amounts and tabulated dissociation constants, but the actual value depends on pH, ionic strength, temperature, Mg^{2+}, ATP, and the apparent binding constants of every competing ligand, so the computed value is only an approximate target. In addition, other components of the solution can carry trace amounts of contaminating calcium, which further offsets the computed value from the actual free [Ca^{2+}]. Therefore it is necessary to develop a system to determine the free calcium concentration in such solutions directly.

1.4. Fluorescence

Fluorescence occurs when a photon from incoming radiation is absorbed by a molecule, exciting it to a higher energy level, followed by the emission of light as the molecule returns to a lower energy state [13]. It is one of two types of photoluminescence, the other being phosphorescence; the two differ in the timescale of emission, with fluorescence ceasing rapidly after the excitation source is removed, while phosphorescent materials continue to emit light for some time after.

The process is most easily summarised with a Jablonski diagram (Fig. 3). At room temperature a molecule resides in the lowest vibrational level of its electronic ground state S_0.

Absorption of a photon of suitable energy promotes one of its electrons to a higher singlet state, most often S_1 or S_2, typically into an excited vibrational sublevel of that state. From there the molecule relaxes very rapidly (on the order of 10^{-12} s) to the lowest vibrational level of S_1 through non-radiative processes collectively known as internal conversion and vibrational relaxation. From the lowest level of S_1 the molecule can return to S_0 by emitting a photon; this radiative transition is fluorescence [14]. The typical fluorescence lifetime is on the order of 10^{-9}–10^{-8} s, several orders of magnitude shorter than phosphorescence, which involves an intermediate triplet state and proceeds on microsecond-to-second timescales.

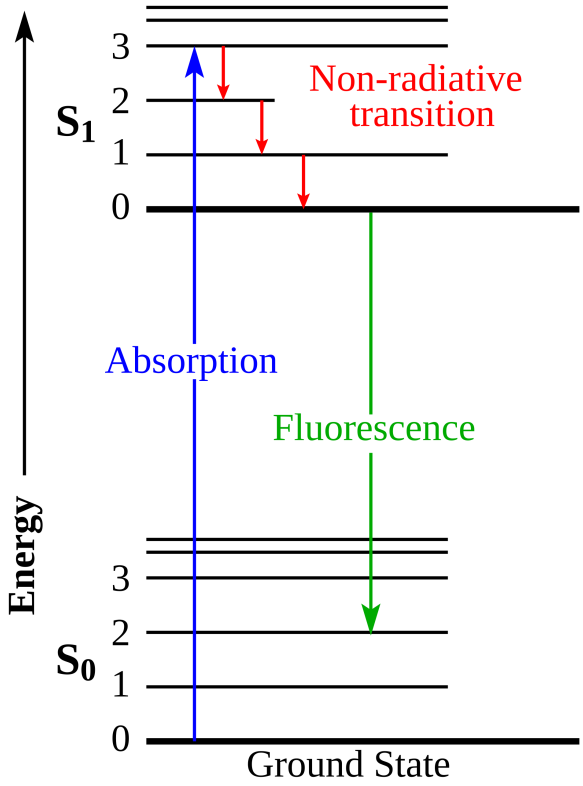

Figure 3: Jablonski diagram showing the principle of fluorescence. Absorption of a photon promotes the molecule from the ground state S_0 to a vibrationally excited level of the first singlet state S_1. Rapid non-radiative vibrational relaxation brings it to the lowest vibrational level of S_1, from which it returns to S_0 by emitting a fluorescence photon of lower energy. Reproduced from [15].

Because part of the absorbed energy is dissipated non-radiatively before emission, the emitted photon carries less energy than the absorbed one. The emission spectrum is therefore shifted to longer wavelengths relative to the absorption spectrum, a phenomenon known as the Stokes shift [16]. The Stokes shift is the property that allows fluorescence to be detected with high sensitivity: the weak emission signal can be optically separated from the much stronger excitation light using wavelength-selective filters.

Two further properties characterize the brightness of a fluorophore [14]. The molar extinction coefficient ε describes how efficiently the molecule absorbs light at a given wavelength, and the fluorescence quantum yield Φ_F is the fraction of absorbed photons that are re-emitted as fluorescence. The product $\varepsilon \cdot \Phi_F$ determines the brightness per molecule. For a dilute, optically thin sample, the measured fluorescence intensity is approximately proportional to

the concentration of the fluorophore, with a proportionality constant that depends on ε, Φ_F, the excitation intensity, and the geometry and sensitivity of the detector.

For calcium indicators such as Cal-590, the quantum yield depends on whether the dye has Ca^{2+} bound to its BAPTA chelating group. Binding of Ca^{2+} increases Φ_F by a large factor without substantially shifting the emission wavelength, so the integrated emission intensity at a fixed wavelength band reports on the fraction of dye in the bound form [17]. This is the property used in the present work.

1.5. Determining free calcium in buffered solutions

Force measurements of the kind described in Section 1.3 require the cardiomyocytes to be exposed to solutions in which the free Ca^{2+} concentration is set to a stable value across a physiological range. At the low concentrations involved, free calcium cannot be set directly by adding a known amount of calcium: small amounts of contamination or pipetting error shift the free concentration significantly. The solutions are therefore buffered with a calcium chelator such as EGTA, which holds the free calcium at a level determined by the chelator equilibrium. The total calcium needed to reach a desired free concentration is typically calculated using a chelator calculator such as MaxChelator or PyChelator [18], of which several variants exist. The results vary depending on the underlying K_d assumptions and buffer composition. In most laboratories the final mixed solutions are not verified after preparation, and the calculated free calcium is taken to be the actual value. The consequences of this are visible in practice: previous force–calcium measurements showed force rising from 0.5 µM [9], whereas comparable preparations in literature typically show force rising around 1 µM [19], suggesting that the calcium concentrations in some solutions may have been incorrectly estimated.

1.5.1. Calcium chelators and the dissociation constant

A calcium chelator is a molecule that binds Ca^{2+} reversibly. When added to a solution in excess relative to its binding affinity, the chelator captures most of the calcium in the solution and acts as a buffer, holding free Ca^{2+} at a level set by the equilibrium between bound and unbound forms.

EGTA (ethylene glycol-bis(β-aminoethyl ether)-N,N,N',N'-tetraacetic acid) is the standard chelator for buffering Ca^{2+} in physiological-strength solutions. Its dissociation constant for Ca^{2+} is approximately 0.2 µM under typical buffer conditions [20]. EGTA binds Mg^{2+} much more weakly than Ca^{2+}, so it selectively controls free Ca^{2+} in solutions that contain physiological amounts of magnesium. EGTA-buffered solutions have been used in cardiac muscle studies since the 1970s, as seen in the work of Fabiato and Fabiato on skinned cardiac cells [2].

The behaviour of any chelator–calcium system can be described by a single reversible bind-

ing reaction. For a calcium ion and a chelator X,

$$\mathrm{Ca}^{2+} + X \underset{k_{\mathrm{off}}}{\overset{k_{\mathrm{on}}}{\rightleftharpoons}} \mathrm{Ca}X, \tag{1}$$

where k_{on} is the association rate constant and k_{off} the dissociation rate constant. By the law of mass action, the bound complex evolves as

$$\frac{\mathrm{d}[\mathrm{Ca}X]}{\mathrm{d}t} = k_{\mathrm{on}}\,[\mathrm{Ca}^{2+}]\,[X] - k_{\mathrm{off}}\,[\mathrm{Ca}X]. \tag{2}$$

At equilibrium the forward and reverse rates are equal, so the net rate is zero, and rearrangement gives the dissociation constant

$$K_d \;=\; \frac{k_{\mathrm{off}}}{k_{\mathrm{on}}} \;=\; \frac{[\mathrm{Ca}^{2+}]\,[X]}{[\mathrm{Ca}X]}. \tag{3}$$

A smaller K_d corresponds to stronger binding. Combined with the conservation of total chelator, $[X]_{\mathrm{tot}} = [X] + [\mathrm{Ca}X]$, Eq. (3) gives the bound fraction as a function of free calcium,

$$\frac{[\mathrm{Ca}X]}{[X]_{\mathrm{tot}}} \;=\; \frac{[\mathrm{Ca}^{2+}]}{K_d + [\mathrm{Ca}^{2+}]}. \tag{4}$$

This is a sigmoid in $[\mathrm{Ca}^{2+}]$ on a logarithmic axis, with half-saturation at $[\mathrm{Ca}^{2+}] = K_d$ (Fig. 4).

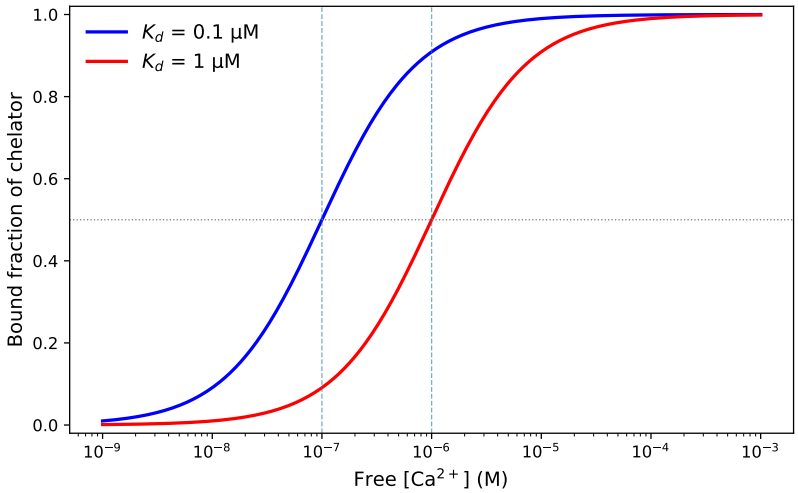

Figure 4: Bound fraction of a chelator as a function of free calcium concentration on a logarithmic axis (Eq. (4)). Half of the chelator is bound at $[\mathrm{Ca}^{2+}] = K_d$. Curves are shown for two values of K_d to illustrate how the dissociation constant shifts the position of the transition.

In a buffered solution, the free calcium concentration at any total calcium can therefore be calculated if the K_d of the chelator and its total concentration are known. The reported K_d of EGTA, however, depends on ionic strength, pH, and temperature, and tabulated values from different sources can disagree by a factor of two or more [21]. The manufactured chemical itself is also typically not 100% pure, and water of crystallisation accounts for several percent of the apparent mass [21]. Both effects contribute to systematic uncertainty in any calculation of free calcium from total amounts.

1.5.2. Measuring free calcium

The uncertainties in the calculated free Ca^{2+} concentration can in principle be addressed by measuring it experimentally. Two methods are available, although neither is routinely used in most laboratories that depend on buffered calcium solutions.

The first method is using a Ca^{2+} selective electrode that measures free calcium directly through the membrane potential that develops across an ion-selective membrane in contact with the solution. Ca^{2+}-selective electrodes have a limited sensitivity range: they give a reliable reading only above a lower detection limit, typically in the range of about 1 to 10 µM depending on the electrode. Below this limit the readings become unreliable, and small voltage errors lead to large errors in $[\mathrm{Ca}^{2+}]$. To work at lower concentrations, the electrode is used to follow EGTA titrations: free $[\mathrm{Ca}^{2+}]$ is read only at the high-calcium end, where the electrode is reliable, and the K_d of EGTA is obtained from the shape of the titration curve. Using this method, Matsuda and Yagi [22] reported apparent EGTA K_d values ranging from 0.238 µM at pH 7.32 to 1.59 µM at pH 6.80 (20 °C, 0.1 M KCl).

The alternative is to use a fluorescent calcium indicator, a small organic molecule whose fluorescence changes upon Ca^{2+} binding and reports indirectly on free $[\mathrm{Ca}^{2+}]$. Indicators are available as membrane-impermeant salts for measurements in solution and in permeabilised preparations, and as acetoxymethyl (AM) esters that cross the cell membrane and become trapped in the cytosol for live-cell imaging of calcium transients. The fluorescence can be measured either with a fluorescence microscope or with a fluorescence spectrometer, which records the full emission spectrum and is well suited to calibration experiments because the emission can be integrated over a defined wavelength band. Each fluorescent indicator consists of two functional parts: a calcium-binding group, usually based on the chelator BAPTA, and a fluorophore whose photophysical properties depend on whether the binding group is empty or occupied [23, 24]. Without calcium the indicator is dim; with calcium bound, fluorescence increases by a large factor. Nanomolar concentrations of indicator are therefore sufficient to report on free $[\mathrm{Ca}^{2+}]$ in the surrounding solution or cytosol.

Indicators are commonly grouped into ratiometric and non-ratiometric classes. Ratiometric dyes such as Fura-2 shift their excitation or emission spectrum upon Ca^{2+} binding, allowing the ratio of intensities at two wavelengths to be used as the calcium-dependent signal. This ratio is independent of dye concentration and excitation intensity. Non-ratiometric dyes such as Fluo-4, Fluo-3, and Cal-590 instead change only their fluorescence intensity at a single wavelength upon Ca^{2+} binding. They are simpler to use because they require only a single excitation wavelength and standard visible-light optics, rather than the UV excitation and rapid wavelength switching needed for ratiometric dyes. They also offer brighter signals, but require careful calibration of the absolute fluorescence response, since the intensity at a single wavelength depends on dye concentration, excitation intensity, and detector sensitivity in addition to calcium concentration [25, 17].

The dye used in this experiment is Cal-590, a red-shifted, non-ratiometric Ca^{2+} indicator

based on the BAPTA chelator. The red-shifted excitation and emission of Cal-590 lie outside the range of typical cellular autofluorescence, which is concentrated in the blue-green region used by older indicators such as Fluo-4. Red-shifted indicators are therefore preferred for live-cell imaging where autofluorescence would otherwise reduce the signal-to-noise ratio [25, 26].

Like the K_d of EGTA, the dissociation constant of a fluorescent indicator depends on ionic strength, pH, temperature, and on dye batch and purity. Tran et al. [21] measured K_d values for several common BAPTA-based indicators in solutions designed to mimic intracellular conditions and reported substantial differences from manufacturer values. For fluo-4FF, the in-situ value of 23 µM differed from the manufacturer-reported 9.7 µM by more than a factor of two; similar discrepancies were found for OGB-6F and fluo-5F. The authors attributed these differences to the strong dependence of BAPTA-based affinity on ionic strength and to inaccuracies in the values of K_d for the calibrating buffer assumed by widely used software tools. Reliable quantitative use of a fluorescent indicator therefore requires in-situ calibration in conditions that match the experiment in which the indicator will be used.

The aim of this work is therefore to develop a fluorescence-based model that determines $K_{d,\mathrm{EGTA}}$ and $K_{d,\mathrm{dye}}$ under the buffer conditions used for cardiomyocyte force measurements, so that the free calcium concentration in such solutions can be calculated reliably from known total concentrations.

2. Methods

2.1. Model

The model was developed iteratively, starting from a single dye–calcium equilibrium and adding components until the fitting procedure recovered the input parameters from synthetic data. Successive iterations introduced EGTA as a second calcium-binding species, included the fluorescence model in the linear form of Eq. (17), and added a calcium offset to absorb trace contamination of the stock solutions. Because a single titration series does not give enough information to determine both $K_{d,\mathrm{dye}}$ and $K_{d,\mathrm{EGTA}}$, the final formulation fits multiple EGTA series simultaneously.

2.1.1. Model description

Reaction scheme. The fluorescence signal measured arises from a calcium-sensitive dye that changes its emission intensity upon binding Ca^{2+}. In addition to the dye, the solutions contained the calcium chelator EGTA, which competes with the dye for the available free Ca^{2+}. The system is therefore described by two reversible binding reactions:

$$\mathrm{Dye} + \mathrm{Ca}^{2+} \underset{k_{\mathrm{off,Dye}}}{\overset{k_{\mathrm{on,Dye}}}{\rightleftharpoons}} \mathrm{CaDye}, \tag{5}$$

$$\mathrm{EGTA} + \mathrm{Ca}^{2+} \underset{k_{\mathrm{off,EGTA}}}{\overset{k_{\mathrm{on,EGTA}}}{\rightleftharpoons}} \mathrm{CaEGTA}. \tag{6}$$

Here k_{on} and k_{off} denote the association and dissociation rate constants of each binding partner, respectively. At thermodynamic equilibrium, their ratio defines the dissociation constant:

$$K_d = \frac{k_{\mathrm{off}}}{k_{\mathrm{on}}}. \tag{7}$$

A smaller K_d indicates stronger binding. The dissociation constants $K_{d,\mathrm{dye}}$ and $K_{d,\mathrm{EGTA}}$ are the key parameters, as they determine how calcium is distributed between the dye, EGTA, and the free pool at any given total calcium concentration.

Differential equations. Denoting the concentrations of the five variables as the state vector

$$\mathbf{y} = \Big[\,[\mathrm{Ca}^{2+}],\ [\mathrm{CaDye}],\ [\mathrm{Dye}],\ [\mathrm{CaEGTA}],\ [\mathrm{EGTA}]\,\Big], \tag{8}$$

where CaDye and CaEGTA are bound complexes and the rest are free species. The reaction rates for the two binding reactions are

$$v_{\text{dye}} = k_{\text{on,Dye}}\,[\text{Ca}^{2+}][\text{Dye}] - k_{\text{off,Dye}}\,[\text{CaDye}], \tag{9}$$

$$v_{\text{EGTA}} = k_{\text{on,EGTA}}\,[\text{Ca}^{2+}][\text{EGTA}] - k_{\text{off,EGTA}}\,[\text{CaEGTA}]. \tag{10}$$

Which yields the following system of ordinary differential equations (ODEs):

$$\frac{d\,[\text{Ca}^{2+}]}{dt} = -\big(v_{\text{dye}} + v_{\text{EGTA}}\big), \tag{11}$$

$$\frac{d\,[\text{CaDye}]}{dt} = \quad v_{\text{dye}}, \tag{12}$$

$$\frac{d\,[\text{Dye}]}{dt} = -v_{\text{dye}}, \tag{13}$$

$$\frac{d\,[\text{CaEGTA}]}{dt} = \quad v_{\text{EGTA}}, \tag{14}$$

$$\frac{d\,[\text{EGTA}]}{dt} = -v_{\text{EGTA}}. \tag{15}$$

This formulation conserves total dye, $[\text{Dye}]_{\text{total}} = [\text{Dye}]+[\text{CaDye}]$, and total EGTA, $[\text{EGTA}]_{\text{total}} = [\text{EGTA}] + [\text{CaEGTA}]$, throughout the integration.

Initial conditions and numerical solution. The model above is a system of coupled ODEs describing how calcium, EGTA, and dye redistribute among free and bound forms. To compare it with the measured fluorescence, which reports the equilibrium state reached after each calcium addition, the system is integrated forward in time from a defined starting point until the concentrations stabilize. At $t = 0$, all calcium is taken to be free and all binding sites unoccupied, giving the initial conditions

$$\mathbf{y}(0) = \Big[\,[\text{Ca}^{2+}]_{\text{total}},\ 0,\ [\text{Dye}]_{\text{total}},\ 0,\ [\text{EGTA}]_{\text{total}}\,\Big]. \tag{16}$$

Fluorescence model. The measured intensity at a fixed emission band can be written as a linear combination of contributions from the free and calcium-bound forms of the dye, plus a background offset:

$$F \;=\; q_{\text{free}}\,[\mathrm{Dye}] \;+\; q_{\text{bound}}\,[\mathrm{CaDye}] \;+\; \gamma, \tag{17}$$

where q_{free} and q_{bound} are the brightness coefficients of the two forms and γ accounts for residual background. In the fit, this expression is evaluated at the steady-state concentrations

$[\mathrm{Dye}]_{\mathrm{ss}}$ and $[\mathrm{CaDye}]_{\mathrm{ss}}$ obtained from the ODE system above. Because the dye used (Cal-590) is strongly fluorescent only in the calcium-bound state, $q_{\mathrm{bound}} \gg q_{\mathrm{free}}$ and the signal is dominated by $[\mathrm{CaDye}]_{\mathrm{ss}}$. Both terms are nonetheless retained in the model to avoid bias in the fitted parameters.

2.1.2. Parameter estimation

The free parameters of the model are

$$\boldsymbol{\theta} = \Big(K_{d,\mathrm{EGTA}},\ K_{d,\mathrm{dye}},\ q_{\mathrm{free}},\ q_{\mathrm{bound}},\ \gamma,\ \Delta[\mathrm{Ca}^{2+}]\Big), \tag{18}$$

where $\Delta[\mathrm{Ca}^{2+}]$ is a small additive calcium offset that accounts for residual free calcium present in nominally calcium-free stock solutions. Parameter estimation was carried out by minimising the sum of squared residuals between the model-predicted and experimentally observed fluorescence values across all titration steps and all EGTA conditions simultaneously:

$$\hat{\boldsymbol{\theta}} \ = \ \arg\min_{\boldsymbol{\theta}} \ \sum_{i=1}^{N} \Big[F_{\mathrm{pred}}\Big([\mathrm{Ca}^{2+}]_i + \Delta[\mathrm{Ca}^{2+}],\ [\mathrm{EGTA}]_i,\ [\mathrm{Dye}]_i;\ \boldsymbol{\theta}\Big) - F_{\mathrm{obs},i} \Big]^2, \tag{19}$$

where the index i runs over all N data points across the three EGTA concentrations.

2.1.3. Implementation

The model was implemented in Python v3.13.5 using the `numpy`, `scipy` and `pandas` packages. The forward rate constants were set to $k_{\mathrm{on,dye}} = 10^6\ \mathrm{M}^{-1}\,\mathrm{s}^{-1}$ and $k_{\mathrm{on,EGTA}} = 10^4\ \mathrm{M}^{-1}\,\mathrm{s}^{-1}$, and the reverse rates were obtained from $k_{\mathrm{off}} = k_{\mathrm{on}} K_d$. The ODE system (Eqs. 11–15) was integrated from $t = 0$ to $t = 100\ \mathrm{s}$ using `scipy.integrate.solve_ivp` with the LSODA solver with absolute and relative tolerances of 10^{-8}. The final concentrations of free and bound dye were then used in Eq. (17) to compute the predicted fluorescence at each titration point. Fitting was done with `scipy.optimize.least_squares` using its default trust-region method. The fit was initialized at $K_{\mathrm{d,EGTA}} = 0.2\ \mu\mathrm{M}$, $K_{\mathrm{d,dye}} = 0.2\ \mu\mathrm{M}$, $q_{\mathrm{free}} = 1.0$, $q_{\mathrm{bound}} = 5 \times 10^4$, $\gamma = 0$, and $\Delta[\mathrm{Ca}^{2+}] = 0$, with all parameters constrained to positive values and $\Delta[\mathrm{Ca}^{2+}]$ upper bound at $200\ \mu\mathrm{M}$. The concentrations for total calcium, dye and EGTA were read from the input data, and the residuals between predicted and measured fluorescence were minimised simultaneously across all three EGTA series.

2.1.4. Simulated data

To verify that the fitting procedure can reliably recover the true parameters, it was first applied to synthetic data generated by a python simulation which computes the expected fluorescence at each point of the calcium titration using the ODE model with set parameters. If the optimization returns values close to those used to generate the data, the fitting procedure is working correctly and the data contains enough information to determine all free parameters. The simulation also serves as a tool for planning the experiment: by generating synthetic fluorescence curves with different numbers of calcium titration points and different spacing between them, one can determine how many measurements are needed and how they should be distributed to obtain a well-defined sigmoidal curve to fit to.

Two types of synthetic data were tested: one without any added noise, and one where Gaussian noise with a coefficient of variation of 1.5% was added to each data point to mimic realistic measurement noise from a fluorimeter. In both cases, the fitted values were compared to the set parameters to confirm that the procedure recovers them accurately.

2.2. Experiments

2.2.1. Solutions

A 137.8 mM EGTA stock solution was prepared in 20 mM HEPES buffer and the pH was adjusted to 7.1 using KOH and HCl. Cal-590 (potassium salt) was prepared as a 25 μM working solution. A 100 mM $CaCl_2$ stock solution was also prepared.

2.2.2. Fluorescence spectrometry

Fluorescence measurements were performed using a spectrofluorophotometer (RF-5301PC, Shimadzu) thermostatted to 23°C. Samples were excited at 574 nm and emission was collected at 580-610 nm. The fluorescent calcium indicator Cal-590 was used in the potassium salt form, which is membrane-impermeant and appropriate for measurements in solution. The dye has a manufacturer-reported dissociation constant of 0.561 µM, an excitation maximum at approximately 574 nm and an emission maximum at approximately 588 nm [17]. Three distinct EGTA concentration series selected using the model were measured independently in a dedicated cuvette. Before each measurement series, the cuvette was filled with 2 ml of HEPES buffer solution and the fluorescence was recorded to account for any background signal of the buffer, which was later subtracted from all measurements. 50 nM of the indicator Cal-590 was then added, and the fluorescence was recorded to establish the dye baseline without Ca^{2+} and EGTA. Next, EGTA was added to the necessary concentration and the fluorescence was recorded again to check that the signal had gone down. Once the base solution was prepared, incremental additions of $CaCl_2$ were done by pipetting from a

100 mM stock solution according to the titration protocol. Fluorescence was recorded after each addition until the solution was fully saturated.

2.2.3. Data preparation

Raw fluorescence emission spectra were recorded as a function of wavelength for each step of the calcium titration. Python was used to parse the spectral data files and reduce each full emission spectrum to a single scalar fluorescence value. This was done by numerical integration of the spectral intensity over a fixed emission band of 585–592.5 nm using the trapezoidal rule. Prior to integration, the blank spectrum — measured in buffer solution without dye under otherwise identical conditions — was subtracted from each sample spectrum to remove background contributions. Total calcium, EGTA, and dye concentrations for each titration step were extracted automatically from the filenames used during data acquisition. The processed data was stored as a table containing one row per measurement, with columns for total calcium concentration, extracted fluorescence, dye concentration, and EGTA concentration.

3. Results and discussion

3.1. Model selection

The final model (Section 2.1.1), fitted simultaneously to three EGTA series with separate parameters for the bound and free dye brightness and a calcium offset, is the simplest formulation that reproduced the synthetic data across all three conditions.

3.2. Simulated data

3.2.1. Fluorescence curves

Before the experiments were carried out, simulations of the expected fluorescence intensity were performed to assess how many calcium titration points were needed to accurately capture the sigmoidal transition of the curve and to verify that the fitting procedure is capable of recovering set parameter values from synthetic data. The simulation uses the same model as the fitting procedure (described in section 2.1.1). For each combination of EGTA concentration and total calcium, steady-state concentrations were obtained by integrating the coupled binding kinetics to equilibrium, and the predicted fluorescence was computed from Eq. (17). The simulation used the manufacturer-reported value of $K_{\mathrm{d,dye}} = 0.561\ \mu\mathrm{M}$ for Cal-590 [17] and the literature value of $K_{\mathrm{d,EGTA}} = 0.238\ \mu\mathrm{M}$ [20]. The brightness coefficients were set to $q_{\mathrm{free}} =\sim 0$ and $q_{\mathrm{bound}} = 5.5 \times 10^4\ \mathrm{a.u.}\ \mu\mathrm{M}^{-1}$, the background offset and calcium contamination were set to zero, and the dye concentration was fixed at $50\ \mathrm{nM}$.

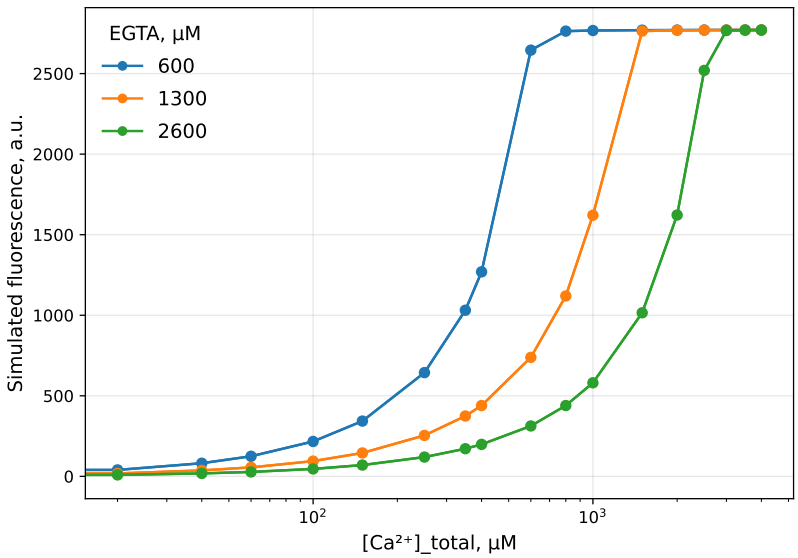

Figure 5: Simulated fluorescence as a function of total calcium concentration for EGTA concentrations of 600, 1300 and 2600 µM, computed using literature parameter values prior to the experiment. The simulation was used to select the EGTA concentrations and the calcium titration grid. Dye concentration 50 nM; $K_{\mathrm{d,dye}} = 0.561$ µM; $K_{\mathrm{d,EGTA}} = 0.238$ µM. The x-axis is on a logarithmic scale.

The simulations served several purposes in designing the experiment. First, they were used to select EGTA concentrations that place the steep transition across a practical range of total calcium. The three concentrations chosen — 600, 1300 and 2600 µM — were found to place the transitions at sufficiently separated positions on the total-calcium axis while remaining practical experimentally, as shown in Fig. 5.

Second, the simulations were used to define the calcium titration grid. A non-uniform spacing was chosen: denser steps at low calcium, where the fluorescence rises most steeply, progressively coarser steps through the mid-range, and larger jumps as the curve approaches its plateau. This concentrates measurements where the signal carries the most information about the binding parameters, without requiring a large number of titration points.

3.2.2. Fitting to simulated data

To verify that the fitting procedure can reliably recover the true parameter values, it was first applied to synthetic data generated by the simulation.

Two variants of synthetic data were tested. In the first variant, noise-free curves were used. In the second variant, Gaussian noise proportional to the fluorescence value was added to the simulated curves, with a variation of 1.5%, to mimic the level of measurement noise expected from a fluorescence spectrometer. Both variants used the three EGTA series and a non-uniform calcium grid, and the resulting plots are shown in Fig. 6.

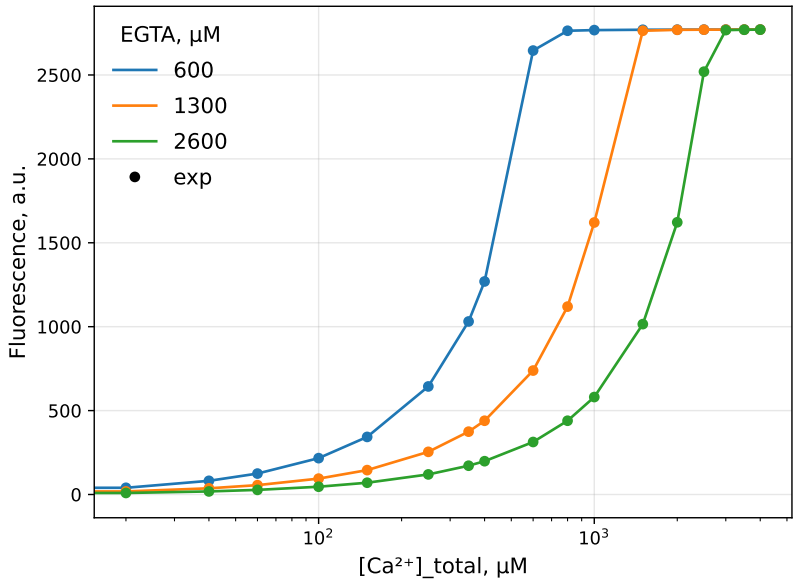

(a) Fit to noise-free simulated fluorescence.

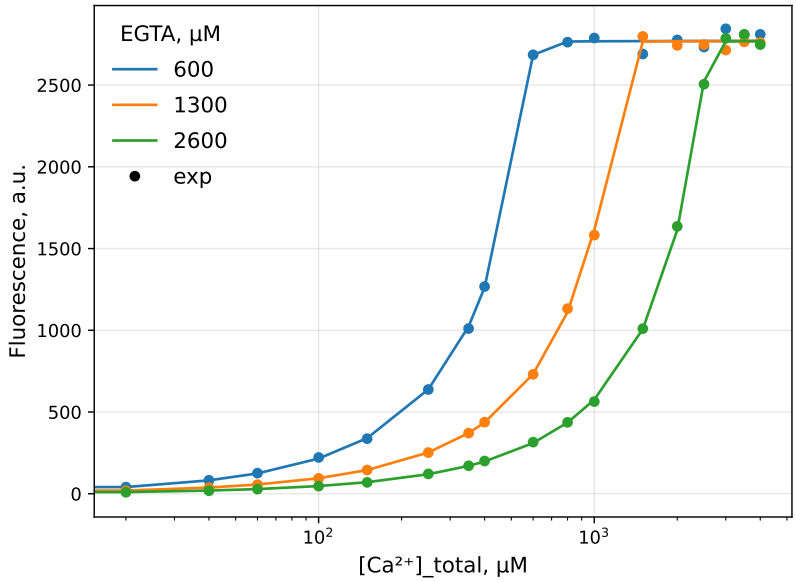

(b) Fit to simulated fluorescence with 1.5% Gaussian noise.

Figure 6: Fitting procedure applied to simulated data. In both panels, circles show simulated fluorescence and lines show the fitted model for EGTA = 600, 1300 and 2600 µM. Dye concentration 50 nM. The x-axes are on a logarithmic scale.

The fitted parameters recovered from the noise-free and noise-added synthetic datasets are compared with the true values in Table 1. In both cases, the recovered $K_{\mathrm{d,EGTA}}$ and $K_{\mathrm{d,Dye}}$ match closely with the input values, and q_{bound} is recovered essentially exactly. The recovered $\Delta[\mathrm{Ca}^{2+}]_0$ is consistent with its true value of zero.

The recovered q_{free} deviates substantially from the true value. This happens because $q_{\mathrm{free}} \ll q_{\mathrm{bound}}$ and the free-dye concentration is at most $[\mathrm{Dye}]_{\mathrm{total}} = 50$ nM, so the $q_{\mathrm{free}}[\mathrm{Dye}]_{\mathrm{ss}}$ term contributes very little to the total fluorescence. Changing q_{free} therefore barely affects the

predicted signal, and the optimizer can return any value within its bounds. The background offset γ is also poorly constrained: it shifts the baseline in the same way as q_{free}, so the data cannot separate the two, and under noise γ absorbs residual variance instead of converging to its true value. The remaining parameters ($K_{\mathrm{d,EGTA}}$, $K_{\mathrm{d,Dye}}$, q_{bound}, $\Delta[\mathrm{Ca}^{2+}]_0$) set the shape and position of the curve and are recovered correctly. Adding 1.5% noise introduces only small deviations in the well-constrained parameters, showing that the fitting procedure is robust to noise.

The recovery of the input parameters from both noise-free and noisy synthetic data suggests that the model and fitting procedure are internally consistent: when the data contains enough information to constrain a parameter, the optimiser returns its true value. This provides a useful baseline for interpreting the experimental fits: if the fitted parameters from the measured data differ noticeably from literature values, the difference is more likely to reflect properties of the data or of the experimental system than limitations of the fitting procedure itself.

Table 1: Comparison of parameter values used to generate the simulated data and the values recovered by the fitting procedure, for noise-free and noise-added ($\sigma = 1.5\%$) synthetic datasets. q_{free} and γ are poorly constrained by the data (see text) and are therefore not expected to be recovered accurately. Uncertainties are omitted where the fit could not estimate them reliably.

Parameter	True value	Recovered (no noise)	Recovered (1.5% noise)
$K_{\mathrm{d,EGTA}}$ (µM)	0.238	$0.238 \pm 1 \times 10^{-7}$	0.25 ± 0.10
$K_{\mathrm{d,dye}}$ (µM)	0.561	$0.561 \pm 2 \times 10^{-7}$	0.58 ± 0.20
q_{free} (a.u. µM^{-1})	~ 0	$4.6 \times 10^{-4} \pm 0.6$	8.6×10^{-2}
q_{bound} (a.u. µM^{-1})	5.5×10^4	$5.5 \times 10^4 \pm 0.6$	5.6×10^4
γ (a.u.)	~ 0	$2.7 \times 10^{-6} \pm 3 \times 10^{-2}$	1.1
$\Delta[\mathrm{Ca}^{2+}]_0$ (µM)	0	$2.3 \times 10^{-7} \pm 3 \times 10^{-6}$	$8 \times 10^{-11} \pm 3 \times 10^{-6}$

3.3. Experimental data

3.3.1. Fluorescence measurements

Fluorescence measurements were carried out using a fluorescence spectrometer, with samples held in cuvettes. Each cuvette was measured with a fixed dye concentration of 50 nM and a fixed EGTA concentration, while total calcium was increased from 20 µM to 2500 µM. The EGTA concentrations used were 600 µM, 1300 µM and 2600 µM, matching the concentrations used in the simulation. The last data point in the 1300 µM titration series had to be excluded due to the spectrofluorometer overheating and being unable to measure an accurate signal. The resulting experimental conditions are summarised in Table 2.

Table 2: Summary of measurement conditions for the three cuvettes. All measurements were performed in HEPES buffer with 50 nM dye. $[\mathrm{Ca}^{2+}]_{\mathrm{total}}$ range indicates the lowest and highest total calcium concentration.

Cuvette	EGTA (µM)	$[\mathrm{Ca}^{2+}]_{\mathrm{total}}$ range (µM)
1	600	20–2500
2	1300	20–1500
3	2600	20–2500

Before each titration, three background spectra were recorded to establish the starting state of the solution (Fig. 7a). The HEPES buffer alone gave a near zero signal across the measured wavelength range, confirming that the buffer alone does not contribute to the fluorescence. Adding 50 nM Cal-590 produced a clear emission peak near 588 nm, even though no calcium had been added. Cal-590 is designed to be dim in the absence of calcium, so a signal of this magnitude indicates that trace calcium was already present in the solution, most likely introduced through the HEPES buffer or the dye stock. Adding EGTA to the same solution suppressed the dye signal almost completely. This confirms that trace calcium is present in the stock solutions and that EGTA is needed to bring the fluorescence down.

An example spectrum recorded during the calcium titration is shown in Fig. 7b. The shaded band (585–592.5 nm) indicates the wavelength range over which each spectrum was integrated to produce the scalar fluorescence values used in the subsequent analysis.

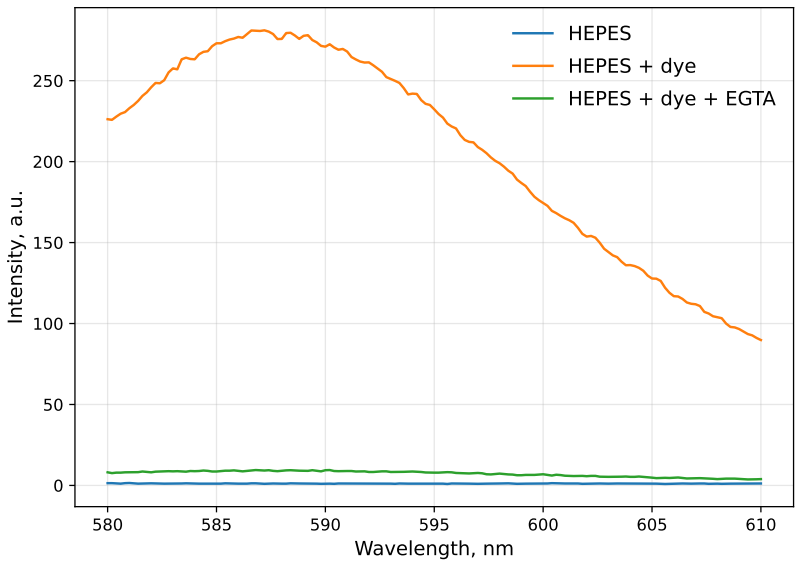

(a) Background spectra recorded before the titration: HEPES buffer alone, HEPES with 50 nM Cal-590 added, and HEPES with dye and 600 µM EGTA added.

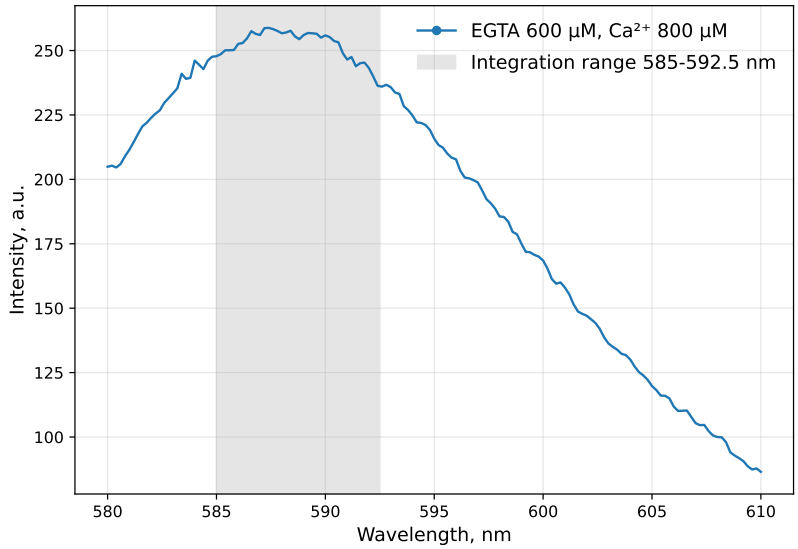

(b) Example of raw data of measured fluorescence intensity as a function of wavelength for one titration. EGTA 600 µM, total calcium 800 µM and dye concentration 50 nM. The shaded area is the range integrated to reduce each full emission spectrum to a single scalar fluorescence value.

Figure 7: Raw fluorescence spectra recorded during a single titration series.

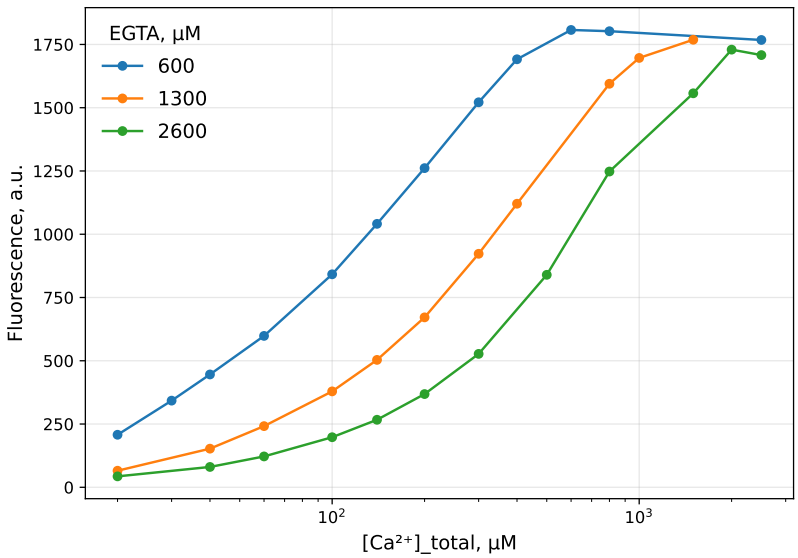

Figure 8: Measured fluorescence as a function of total calcium concentration for the three EGTA concentrations: 600 µM, 1300 µM and 2600 µM. Dye concentration 50 nM. The x-axis is on a logarithmic scale.

As seen in Fig. 8, in all three series, the fluorescence increased steadily with added calcium, as expected from the progressive binding of calcium to the dye. The measured curves follow the sigmoidal shape predicted by the simulation (Fig. 5), but the transitions are less steep than predicted. This is consistent with a higher $K_{d,\text{EGTA}}$ than the literature value used in the simulation, which broadens the calcium range over which the buffer transitions between unbound and saturated. The lowest EGTA series (600 µM) also shows a noticeably higher fluorescence at the first titration points, suggesting that this EGTA concentration was not enough to buffer the trace calcium present in the starting solution. At higher EGTA concentrations the contamination seems to get absorbed and the starting fluorescence is lower.

3.3.2. Fitting to experimental data

The model was initially fitted with both $K_{d,\text{dye}}$ and $K_{d,\text{EGTA}}$ as free parameters, but the optimisation did not return well-defined values for both constants simultaneously. The three EGTA series measured do not provide enough independent constraints to separate them. The measured titration curves also differed slightly in shape from those predicted by the simulation (Fig. 5), which likely reflects a combination of pipetting error, trace calcium contamination of the stocks, and EGTA purity. The fit is also constrained by the limited amount of experimental data available. $K_{d,\text{dye}}$ was therefore fixed at the manufacturer-reported value of 0.561 µM [17], and $K_{d,\text{EGTA}}$ was fitted as a free parameter along with q_{free}, q_{bound}, γ, and $\Delta[\text{Ca}^{2+}]$.

As seen in Table 3 the fitted $K_{d,\text{EGTA}} = 1.89$ µM is much higher than the literature value of 0.238 µM [20] used in the simulation (Section 3.2.2). This kind of difference is not surprising, since the apparent K_d of EGTA depends strongly on pH, ionic strength, and temperature,

and the present measurements were carried out in a buffer that differs from the one used in the original characterisation. Matsuda and Yagi [22] obtained the apparent K_d of EGTA through direct measurements with a Ca^{2+}-selective electrode and obtained values ranging from 0.238 μM at pH 7.32 to 1.59 μM at pH 6.80 (20°C, 0.1 M KCl), showing that values in the range fitted here can occur under slightly different buffer conditions. Tran et al. [21] reported similar deviations from manufacturer-provided values for several BAPTA-based fluorescent indicators measured under intracellular-like conditions, with in-situ K_d values differing from manufacturer values by more than a factor of two in some cases. The same model was also applied to an earlier dataset acquired under comparable conditions and returned a $K_{d,\mathrm{EGTA}}$ of similar magnitude, indicating that the elevated value comes from the experimental conditions rather than the fitting procedure.

The fitted q_{free} and γ are both essentially zero, meaning the unbound dye contributes negligibly to the measured signal. The optimiser was unable to assign meaningful uncertainties to either parameter, which is expected given that $q_{\mathrm{free}} \ll q_{\mathrm{bound}}$ and the free-dye contribution to the total fluorescence is negligible across the entire titration range.

The fitted calcium offset $\Delta[\mathrm{Ca}^{2+}] = 13.1$ μM indicates trace calcium contamination in the nominally calcium-free stock solutions. The offset is small compared with the total calcium concentrations spanned by the titration (20–2500 μM), but comparable in magnitude to the lowest titration points, where the measured fluorescence is systematically higher than the model prediction. Including $\Delta[\mathrm{Ca}^{2+}]$ as a free parameter therefore noticeably improves the fit at the low-Ca end of the curve.

Table 3: Fitted model parameters obtained from the measured dataset. q_{free}, q_{bound}: specific fluorescence yields of free and bound dye; γ: additive background offset; $\Delta[\mathrm{Ca}^{2+}]_0$: fitted calcium background. $K_{\mathrm{d,dye}}$ was fixed at 0.561 μM.

Parameter	Value
$K_{\mathrm{d,EGTA}}$ (μM)	1.89 ± 0.10
q_{free} (a.u. μM^{-1})	~ 0
q_{bound} (a.u. μM^{-1})	$38\,200 \pm 400$
γ (a.u.)	~ 0
$\Delta[\mathrm{Ca}^{2+}]$ (μM)	13.1 ± 3.7

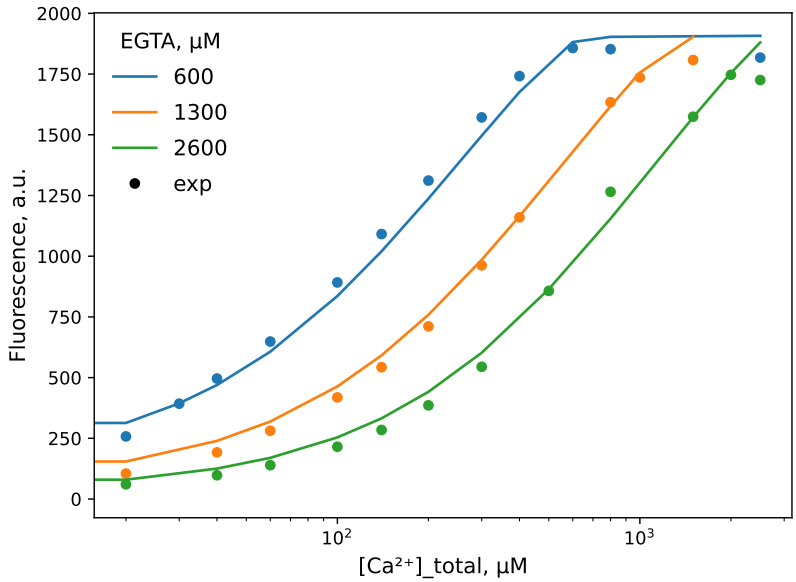

Figure 9: Measured fluorescence (circles) and fitted model (lines) as a function of total calcium concentration for the three cuvettes. Dye concentration 50 nM. The x-axis is on a logarithmic scale.

The fitted curves match the measured data well across all three EGTA concentrations, as shown in Figures 9 and 10. Since the dye fluorescence depends on only the free calcium concentration, if the model calculates free calcium correctly at each EGTA concentration, all three series should fall on the same curve when plotted against free calcium. This is what is observed in Figure 10, supporting the conclusion that the model accounts for EGTA-dependent calcium buffering and that a single set of parameters reproduces the measured fluorescence across all three EGTA conditions.

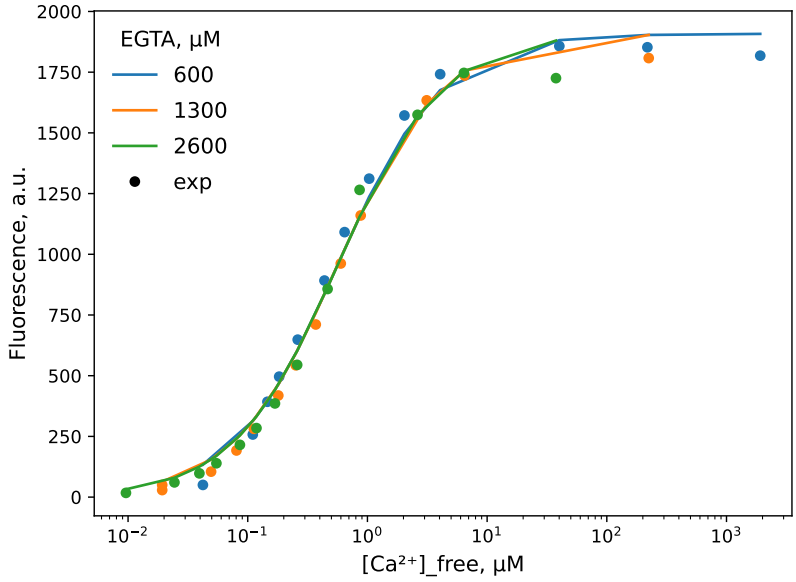

Figure 10: Measured fluorescence (circles) and fitted model (lines) as a function of free calcium concentration for the three EGTA conditions. Dye concentration 50 nM. The x-axis is on a logarithmic scale.

3.4. Current limitations and future directions

The main limitation of the present work is the size and scope of the experimental dataset. Only three EGTA series were measured, each consisting of 12–13 calcium titration points, which is a small sample on which to base a statistical comparison with literature K_d values. The titration experiments themselves proved time-consuming and technically demanding: each series required careful sequential pipetting of microliter-scale volumes from stocks into a 2 mL cuvette, with fluorescence measurement after every addition, and the procedure was sensitive to small experimental inconsistencies such as pipetting error and incomplete mixing between additions. Within the time available for this thesis, the dataset could not be expanded to include replicates of each EGTA series, which would have allowed the reproducibility of the fitted parameters to be assessed directly. The limited size of the dataset also meant that $K_{d,\mathrm{Dye}}$ could not be reliably recovered from the experimental fit and had to be fixed at its manufacturer-reported value, leaving $K_{d,\mathrm{EGTA}}$ as the only dissociation constant determined from the measurements. Expanding the dataset is therefore the most immediate priority for future work.

A second limitation is that the calibration was performed in a simple HEPES buffer rather than in a solution that mimics the intracellular environment in which the dye is ultimately used. Real intracellular solutions for permeabilized cardiomyocyte experiments contain additional components, most notably MgATP and phosphocreatine at millimolar concentrations, which can affect the effective K_d of both EGTA and the dye through ionic-strength effects, competing Mg^{2+} binding to EGTA, and possible interactions with the dye. The K_d values reported here therefore characterize Cal-590 and EGTA under the specific conditions of the calibration buffer; transferring them to physiological measurements would require a separate calibration in a matched intracellular-type solution. A preliminary attempt was made to repeat the calibration in a solution containing Mg^{2+} alongside EGTA and the dye, to approximate the intracellular environment more closely. The measured fluorescence curves showed poor reproducibility between titration points and did not display the clean sigmoidal shape measured in the HEPES-only buffer, so the data were not analysed further. Performing such a calibration is a natural next step and would extend the method developed here to the conditions under which the dye is intended to be used.

Conclusion

The aim of this thesis was to determine the dissociation constants of the chelator EGTA and the calcium indicator Cal-590 from a fluorescence titration experiment. This involved building a kinetic model of calcium binding to the dye and EGTA, implementing a fitting procedure to recover both dissociation constants from fluorescence titration data, and testing the method on synthetic data before applying it to measurements. Several iterations of the model were tested until the final formulation, which fits three EGTA series simultaneously, was reached. The fitting procedure was first validated against simulated data, where it successfully recovered the dissociation constants, both with and without added noise. This confirmed that the procedure works as intended and provided a baseline against which the experimental fits could be interpreted.

The titration experiments were established and repeated until a clean dataset including three EGTA concentrations was obtained. Despite the small size of the dataset, the fit converged and yielded a value of $K_{d,\mathrm{EGTA}}$ under the conditions of the calibration buffer, along with consistent values for the fluorescence parameters of the dye. The dissociation constant of Cal-590 itself could not be reliably determined from the limited dataset and was fixed to the manufacturer-reported value during the experimental fit. Recovering both constants from a single experiment, as the method was designed to do, will therefore require a larger dataset than was possible within the scope of this thesis.

The method will be further developed to enable calibration in intracellular-type solutions, which is the condition under which the dye is ultimately used.

Acknowledgments

I would like to thank my supervisors, Maike Mona Širinov and Marko Vendelin, for their patience and support throughout this work. I am especially grateful to Maike Mona for guiding me through the experimental side, from preparing the solutions to re-teaching me high school chemistry, and to Marko for his help with the mathematical modelling and for helping figure things out whenever something went wrong. I am also grateful to both of them for putting up with me when I got stuck or confused.

References

[1] R. E. Ahmed, T. Tokuyama, T. Anzai, N. Chanthra, and H. Uosaki, "Sarcomere maturation: function acquisition, molecular mechanism, and interplay with other organelles," *Philosophical Transactions of the Royal Society B: Biological Sciences*, vol. 377, p. 20210325, 10 2022.

[2] A. Fabiato and F. Fabiato, "Contractions induced by a calcium-triggered release of calcium from the sarcoplasmic reticulum of single skinned cardiac cells.," *The Journal of Physiology*, vol. 249, no. 3, pp. 469–495, 1975.

[3] D. M. Bers, "Cardiac excitation–contraction coupling," *Nature*, vol. 415, pp. 198–205, jan 2002.

[4] D. A. Eisner, J. L. Caldwell, K. Kistamás, and A. W. Trafford, "Calcium and excitation-contraction coupling in the heart," *Circulation Research*, vol. 121, no. 2, pp. 181–195, 2017.

[5] G. Redel-Traub, S. O. Marx, and A. R. Marks, "Targeting calcium regulation for heart failure and arrhythmia therapeutics: A critical review," *Circulation*, vol. 152, no. 13, pp. 957–970, 2025.

[6] L. Liu, K. Zhou, X. Liu, Y. Hua, H. Wang, and Y. Li, "The interplay between cardiac dyads and mitochondria regulated the calcium handling in cardiomyocytes," *Frontiers in Physiology*, vol. 13, p. 1013817, 2022.

[7] S. Zaffran, L. Kraoua, and H. Jaouadi, "Calcium handling in inherited cardiac diseases: A focus on catecholaminergic polymorphic ventricular tachycardia and hypertrophic cardiomyopathy," *International Journal of Molecular Sciences*, vol. 24, no. 4, p. 3365, 2023.

[8] M. Kalda, *Mechanoenergetics of a Single Cardiomyocyte*. PhD thesis, Tallinn University of Technology, Tallinn, 2015.

[9] M. M. Širinov, "Calcium activation in cardiac muscle: experimental and modelling studies," master's thesis, Tallinn University of Technology, Tallinn, 2025.

[10] P. Peterson, M. Kalda, and M. Vendelin, "Real-time determination of sarcomere length of a single cardiomyocyte during contraction," *American Journal of Physiology-Cell Physiology*, vol. 304, no. 6, pp. C519–C531, 2013.

[11] N. Jepihhina, N. Béraud, M. Sepp, R. Birkedal, and M. Vendelin, "Permeabilized rat cardiomyocyte response demonstrates intracellular origin of diffusion obstacles," *Biophysical Journal*, vol. 101, no. 9, pp. 2112–2121, 2011.

[12] M. M. Širinov, "Design and implementation of a system for single myofibril force measurements," bachelor's thesis, Tallinn University of Technology, Tallinn, 2023.

[13] C. N. Banwell and E. M. McCash, *Fundamentals of Molecular Spectroscopy*. London: McGraw-Hill, 3 ed., 1994.

[14] J. R. Lakowicz, *Principles of Fluorescence Spectroscopy*. New York: Springer, 3 ed., 2006.

[15] Wikimedia Commons, "Jablonski Diagram of Fluorescence Only." `https://commons.wikimedia.org/wiki/File:Jablonski_Diagram_of_Fluorescence_Only-en.svg`, 2009. CC0 Public Domain Dedication; accessed April 2026.

[16] B. Valeur and M. N. Berberan-Santos, *Molecular Fluorescence: Principles and Applications*. Weinheim: Wiley-VCH, 2 ed., 2012.

[17] AAT Bioquest, "Cal-520, cal-590, and cal-630 calcium detection reagents: Product technical information sheet." Technical information sheet, Jan. 2017. Last updated January 2017.

[18] E. Spahiu, E. Kastrati, and M. Amrute-Nayak, "PyChelator: a Python-based Colab and web application for metal chelator calculations," *BMC Bioinformatics*, vol. 25, p. 239, 2024.

[19] K. C. Woulfe, C. Ferrara, J. M. Pioner, J. H. Mahaffey, R. Coppini, B. Scellini, C. Ferrantini, N. Piroddi, C. Tesi, C. Poggesi, and M. Jeong, "A novel method of isolating myofibrils from primary cardiomyocyte culture suitable for myofibril mechanical study," *Frontiers in Cardiovascular Medicine*, vol. 6, p. 12, 2019.

[20] R. Tsien and T. Pozzan, "Measurement of cytosolic free Ca^{2+} with quin2," in *Biomembranes Part S*, vol. 172 of *Methods in Enzymology*, pp. 230–262, Academic Press, 1989.

[21] V. Tran, M. C. H. Park, and C. Stricker, "An improved measurement of the Ca2+-binding affinity of fluorescent Ca2+ indicators," *Cell Calcium*, vol. 71, pp. 86–94, 2018.

[22] S. Matsuda and K. Yagi, "The apparent binding constants of Ca^{2+} to EGTA and heavy meromyosin," *Journal of Biochemistry*, vol. 88, pp. 1515–1520, Nov. 1980.

[23] R. Y. Tsien, "New calcium indicators and buffers with high selectivity against magnesium and protons: design, synthesis, and properties of prototype structures," *Biochemistry*, vol. 19, no. 11, pp. 2396–2404, 1980.

[24] G. Grynkiewicz, M. Poenie, and R. Y. Tsien, "A new generation of Ca^{2+} indicators with greatly improved fluorescence properties," *Journal of Biological Chemistry*, vol. 260, no. 6, pp. 3440–3450, 1985.

[25] M. Collot, C. Loukou, A. V. Yakovlev, C. D. Wilms, D. Li, A. Evrard, A. Zamaleeva, L. Bourdieu, J.-F. Léger, N. Ropert, J. Eilers, M. Oheim, A. Feltz, and J.-M. Mallet, "Calcium rubies: A family of red-emitting functionalizable indicators suitable for two-photon ca2+ imaging," *Journal of the American Chemical Society*, vol. 134, no. 36, pp. 14923–14931, 2012.

[26] M. Monici, "Cell and tissue autofluorescence research and diagnostic applications," *Biotechnology Annual Review*, vol. 11, pp. 227–256, 2005.

Appendices

Appendix 1. Non-exclusive licence

Annex
to Rector's directive No 1-8/17 of 7 April 2020

Non-exclusive licence for reproduction and publication of a graduation thesis[1]

I, Mirtel Toming

1. grant Tallinn University of Technology free licence (non-exclusive licence) for my thesis Mathematical modelling of calcium binding in solution,

supervised by Marko Vendelin and Maike Mona Širinov,

1.1 to be reproduced for the purposes of preservation and electronic publication of the graduation thesis, incl. to be entered in the digital collection of the library of Tallinn University of Technology until expiry of the term of copyright;

1.2 to be published via the web of Tallinn University of Technology, incl. to be entered in the digital collection of the library of Tallinn University of Technology until expiry of the term of copyright.

2. I am aware that the author also retains the rights specified in clause 1 of the non-exclusive licence.

3. I confirm that granting the non-exclusive licence does not infringe other persons' intellectual property rights, the rights arising from the Personal Data Protection Act or rights arising from other legislation.

22.05.2026

[1] *The non-exclusive licence is not valid during the validity of access restriction indicated in the student's application for restriction on access to the graduation thesis that has been signed by the school's dean, except in case of the university's right to reproduce the thesis for preservation purposes only. If a graduation thesis is based on the joint creative activity of two or more persons and the co-author(s) has/have not granted, by the set deadline, the student defending his/her graduation thesis consent to reproduce and publish the graduation thesis in compliance with clauses 1.1 and 1.2 of the non-exclusive licence, the non-exclusive license shall not be valid for the period.*